JOURNAL OF AIRCRAFT
Vol. 40, No. 5, September–October 2003

Dynamic Deformation Measurements of an Aeroelastic Semispan Model

Sharon Suzanne Graves,* Alpheus W. Burner,† John W. Edwards,‡ and David M. Schuster§
NASA Langley Research Center, Hampton, Virginia 23681-2199

The techniques used to acquire, reduce, and analyze dynamic deformation measurements of an aeroelastic semispan wind-tunnel model are presented. Single-camera, single-view video photogrammetry (also referred to as videogrammetric model deformation) was used to determine dynamic aeroelastic deformation of the semispan "models for aeroelastic validation research involving computation" model in the Transonic Dynamics Tunnel at NASA Langley Research Center. Dynamic deformation was determined from optical retroreflective tape targets at five semispan locations located on the wing from the root to the tip. Digitized video images from a charge-coupled device camera were recorded and processed to determine automatically target image plane locations that were then corrected for instrumentation errors. Videogrammetric dynamic data were acquired at a 60-Hz rate for time records of up to 6 s during portions of a flutter/limit-cycle oscillation test at Mach numbers from 0.3 to 0.96. Spectral analysis of the deformation data were used to identify dominant frequencies in the wing motion. The dynamic data will be used in future studies to separate aerodynamic and structural effects and to provide time history deflection data for computational aeroelasticity code evaluation and validation.

Introduction

VIDEO photogrammetry was used to measure dynamic deformation on the models for aeroelastic validation research involving computation semispan model (MAVRIC-I), a business jet wing–fuselage flutter model, in NASA Langley Research Center's Transonic Dynamics Tunnel (TDT). The overall objective of this test is to provide benchmark validation data on a representative configuration that exhibits nonlinear, transonic aeroelastic response, specifically limit-cycle oscillations and buffet onset. Instrumentation included unsteady pressure transducers, accelerometers, and strain gauges. Computational aeroelastic analysis will be conducted in the future as part of a research program to assess and refine state-of-the-art design tools.

The primary objective of this series of MAVRIC tests was to provide detailed experimental wind-tunnel data suitable for computational aeroelasticity (CAE) code evaluation and validation at transonic separation onset conditions. Unsteady pressures and wing responses were obtained for three wingtip configurations: clean, tipstore, and winglet. Traditional flutter boundaries were measured over the range of $M = 0.6$–0.9 and maps of limit-cycle-oscillation (LCO) behavior were made in the range of $M = 0.85$–0.95. The dynamic pressure transducers provide time histories of the pressure distribution on the wing as it encounters the flutter or LCO phenomena. However, these pressures are directly dependent on the motion of the wing. Accurate measurement of the wing motion is a critical item when comparing the unsteady surface pressures with computed results. Modern computational aeroelasticity programs are capable of simultaneously computing both the vehicle motion and dynamic loads on the vehicle. However, accurate simultaneous computation of these components is difficult for highly nonlinear problems such as LCO,[1,2] and it is very beneficial to be able to isolate the various components of the problem. This is where the videogrammetry data are of greatest use. When the model motion using data obtained through the videogrammetric system is specified, the issue of computing the model motion can be eliminated from the computational problem, and a direct comparison of computed and wind-tunnel pressures can be performed. Researchers previously depended on strain gauge and accelerometer data to estimate the wing motion. Videogrammetry provides a significantly more accurate and direct method for obtaining these data.

The intent of this paper is to relate experiences using the videogrammetry technique in a large wind tunnel for dynamic deformation measurements to aid potential users of the technique at the TDT and other facilities. Rather than presenting extensive deformation data, only representative data will be included. The data acquisition procedure and interaction with the facility data acquisition system will be described. This work is part of an overall effort to develop a dynamic model deformation measurement capability up to 1000 Hz.

Model

The MAVRIC-I business jet model, shown in Fig. 1, consists of a structurally flexible wing mounted low on a rigid fuselage. The semispan model is constructed of a stepped thickness aluminum plate planform and covered with end-grain balsa wood to provide the wing contour. The wing, with no twist or dihedral, was designed to flutter in the TDT at dynamic pressures between 100 and 200 lb/ft^2. Initial testing of this model in the early 1990s verified the flutter characteristics of the wing and, in the process, also uncovered large-amplitude nonlinear dynamic response behavior. This LCO occurs in the transonic flight regime well below the wing's flutter boundary and is similar to nonlinear phenomena encountered on some operational aircraft such as the F-16.[1] To further investigate this nonlinearity, the model instrumentation was significantly upgraded by 1) adding 87 in situ dynamic pressure transducers, 2) adding eight accelerometers buried in the wing at four spanwise locations, and 3) incorporating the videogrammetric deformation system to measure the dynamic motion of the model. This new instrumentation complements the original instrumentation suite that included wing root bending, torsion strain gauges, and wingtip accelerometers.

Presented as Paper 2001-2454 at the AIAA 19th Applied Aerodynamics Conference, Anaheim, CA, 11–14 June 2001; received 10 May 2002; revision received 2 October 2002; accepted for publication 19 November 2002.

*Research Engineer, Aerodynamics, Aerothermodynamics and Acoustics Competency, Mail Stop 236; s.s.graves@larc.nasa.gov. Member AIAA.

†Senior Research Engineer, Aerodynamics, Aerothermodynamics and Acoustics Competency, Mail Stop 236; a.w.burner@larc.nasa.gov. Associate Fellow AIAA.

‡Senior Research Engineer, Structures and Materials Competency, Mail Stop 340; j.w.Edwards@larc.nasa.gov. Fellow AIAA.

§Senior Research Engineer, Structures and Materials Competency, Mail Stop 340; d.m.Schuster@larc.nasa.gov. Associate Fellow AIAA.

The model was thoroughly retested in the TDT, and detailed measurements were acquired at numerous flutter and LCO conditions.[3] Figure 2 shows the three wingtip configurations used: clean wingtip (body of revolution), pencil tipstore, and winglet with a 41-deg leading-edge sweep.

TDT

The TDT is a unique national facility dedicated to identifying, understanding, and solving aeroelastic problems. The TDT is specifically dedicated to investigating flutter problems of fixed-wing aircraft. The tunnel is also used to investigate other aeroelastic phenomena such as fixed-wing buffet and divergence. The tunnel is used for studying the use of active controls technologies for both fixed-wing and rotary-wing configurations, clearing new designs from flutter, determining the effects of ground-wind loads on launch vehicles, and providing steady and unsteady aerodynamic pressure data to support CAE and additional fluid dynamics code development and validation. The TDT is a closed-circuit, continuous flow, variable pressure wind tunnel with a 16-ft square test section with cropped corners. The tunnel is capable of testing at stagnation pressures from near zero to atmospheric conditions. Controlled variation of pressure in the tunnel is used to simulate variations in flight altitude. The tunnel is capable of using either air or R-134a as the test medium. Testing in a heavy gas, such as R-134a, has important advantages over testing in air, particularly for aeroelastic models. The R-134a refrigerant is about four times as dense as air, yet has a speed of sound of about half that of air. These advantages include improved model to full-scale similitude, higher Reynolds numbers, easier fabrication of scaled models, reduced tunnel power requirements, and in the case of rotary-wing models, reduced model power requirements. The tunnel can operate up to a Mach number of 1.2 and is capable of maximum Reynolds numbers of about 3×10^6/ft in air and 10×10^6/ft in R-134a.

Fig. 1 MAVRIC-I model mounted on tunnel sidewall.

Videogrammetric Measurement Technique

The videogrammetric measurement technique is an optical method characterized by automated image processing, subpixel resolution, near routine, near real-time measurements, and high data volume with minimum impact to productivity.[4–8] The technique consists of a single-camera, single-view, photogrammetric solution from digital images of targets placed on the wing at known semispan locations. Except for the targets, the technique is nonintrusive. For this application, the thickness of the retroreflective tape targets (0.1 mm) is estimated to have negligible effect on the aeroelastic behavior based on the nearly identical pressure data obtained with targets on as with targets off. When a light source is positioned near the camera, the light retroreflected from the tape targets can greatly exceed that possible with white diffuse targets, resulting in a high-contrast image in which the targets are easily discriminated from the background. Such high-contrast images are amenable to automated image processing.

The basic hardware consists of an instrumentation-grade video-rate Hitachi KP-M1 charge coupled device (CCD) camera, an Epix

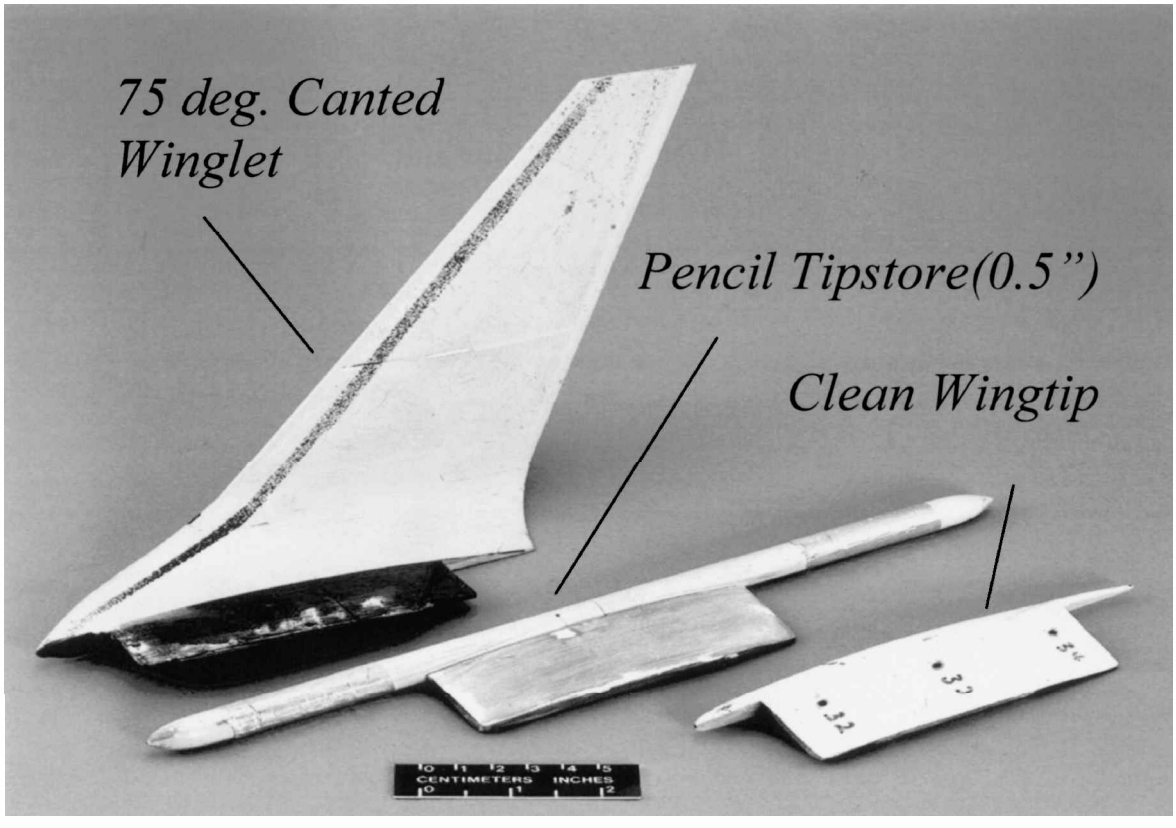

Fig. 2 Wingtip configurations: clean wingtip, pencil tipstore, winglet.

Table 1 Semispan η target positions and diameters

η	Y, in.	D, in.
0.0916	4.87	1.5
0.3513	18.68	1.25
0.4977	26.46	1.25
0.7522	39.99	1.25
0.9656	51.34	1.0

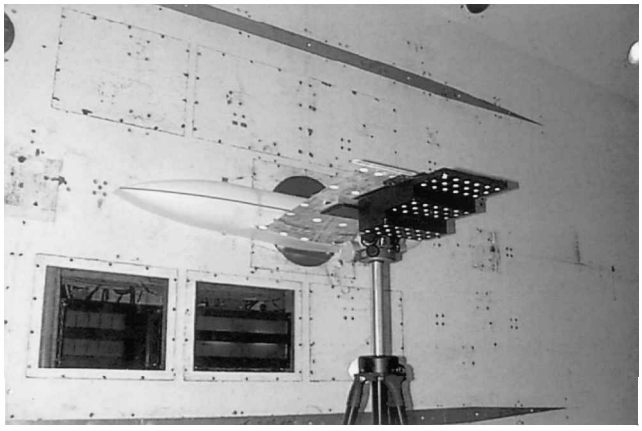

Fig. 3 Calibration plate on model wingtip.

frame grabber board, and a Pentium III-based computer with image acquisition and reduction software. A fiber optic light source is located as close to the camera as possible to take advantage of the retroreflective nature of the optical targets. The camera is positioned to the side and below the model, resulting in an oblique view of the model at an angle of about 32 deg to the horizontal. Targets with diameters D of 1.0–1.5 in. are placed in rows (three targets per row) at five known semispan locations η from near the wing root to near the wingtip (Table 1).

Acquisition and digitization of a live video stream at a nominal 60-Hz rate is triggered by the facility data acquisition system. Once the video sequence is acquired, a blob analysis is used for target detection in the image. A gray-scale centroid calculation with the background level automatically removed provided subpixel precision. Single-view photogrammetry is then used to determine the X (streamwise) and Z (vertical) coordinates in object space, given the known Y (crossflow) coordinates. Z-intercept and slope angles are computed by a linear least-squares fit in X–Z space for each η station along the wing.

Camera Calibration

Camera calibration consists of determining image plane correction parameters for lens distortion and lens alignment to the CCD sensor as well as the determination of the location and pointing angles of the camera in the test section coordinate system. The parameters for image plane corrections are determined in a laboratory before setting up the measurement system in the test section at the TDT.

A calibration fixture consisting of a number of targets with known spatial coordinates was used to determine lens distortion and principal distance (Fig. 3). Only third-order radial distortion and a single term for decentering distortion were found to be statistically significant to warrant their inclusion in the correction parameters. A laser illumination technique was used to determine the photogrammetric principal point and point of symmetry for distortion. Once the measurement system was set up with the proper view of the model, a calibration fixture was aligned to the test section coordinate system to determine the pointing angles and location of the camera via photogrammetric space resection.

Data Reduction

The videogrammetric model deformation (VMD) measurement technique uses photogrammetry to extract two-dimensional images and map them into a three-dimensional object space. The collinearity equations provide a mapping of coordinates between three-dimensional object space and the two-dimensional coordinates in the image plane. The nth target location point $p_n = (x_n, y_n\}^T$ in the image plane is related to a point $P_n = (X_n, Y_n, Z_n\}^T$ in the object space by

$$x_n - x_p + \delta x = -c\frac{m_{11}(X_n - X_c) + m_{12}(Y_n - Y_c) + m_{13}(Z_n - Z_c)}{m_{31}(X_n - X_c) + m_{32}(Y_n - Y_c) + m_{33}(Z_n - Z_c)}$$

$$y_n - y_p + \delta y = -c\frac{m_{21}(X_n - X_c) + m_{22}(Y_n - Y_c) + m_{23}(Z_n - Z_c)}{m_{31}(X_n - X_c) + m_{32}(Y_n - Y_c) + m_{33}(Z_n - Z_c)} \tag{1}$$

The interior orientation of the camera is given by the parameter set (c, x_p, y_p). The exterior orientation of the camera is given by the parameter set $(\omega, \phi, \kappa, X_c, Y_c, Z_c)$, where ω, ϕ, and κ are rotational Euler angles and X_c, Y_c, and Z_c represent the coordinates of the perspective center of the camera in object space. The δx and δy terms are correction terms due to lens distortion. The elements of the rotation matrix in the preceding equations are given by

$$m_{11} = \cos\phi\cos\kappa, \qquad m_{12} = \sin\omega\sin\phi\cos\kappa + \cos\omega\sin\kappa$$

$$m_{13} = -\cos\omega\sin\phi\cos\kappa + \sin\omega\sin\kappa, \qquad m_{21} = -\cos\phi\sin\kappa$$

$$m_{22} = -\sin\omega\sin\phi\sin\kappa + \cos\omega\cos\kappa$$

$$m_{23} = \cos\omega\sin\phi\sin\kappa + \sin\omega\cos\kappa, \qquad m_{31} = \sin\phi$$

$$m_{32} = -\sin\omega\cos\phi, \qquad m_{33} = \cos\omega\cos\phi \tag{2}$$

The local angle α_l at each η station is defined by

$$\alpha_l = -\tan^{-1}(\Delta Z/\Delta X) \tag{3}$$

Local wing twist θ due to aerodynamic loads is defined as[7]

$$\theta = \alpha_i^{\text{on}}(\eta) - \alpha_i^{\text{off}}(\eta) \tag{4}$$

where $\alpha_l^{\text{on}}(\eta)$ and $\alpha_l^{\text{off}}(\eta)$ are the local angles α_l in the wind-on and wind-off cases at the same semispan location η.

In a single camera VMD system, a solution (X, Y, Z) to the collinearity equations from a single set of image coordinates (x, y) is not possible unless additional information is provided. Because motion is basically confined to the pitch plane during this test, the spanwise locations Y of the targets are fixed so that the number of unknowns reduces to two, namely, X and Z.

Uncertainty

The uncertainty of the VMD technique is related to the uncertainties in target centroid measurements, camera calibration, and data reduction (calculations of coordinates, twist, and bending). The uncertainty in target centroid measurement is associated with camera noise, centroid calculation schemes, target size, and spatial quantization of a CCD sensor. The random errors associated with the camera noise can be collectively represented by the centroid variations for spatially fixed targets. Typically these centroid variations are on the order of 0.01 pixel or less for static objects in a laboratory environment. These centroid uncertainties limit the accuracy of VMD measurements in the object space.

The VMD system resolution depends on the fraction of the image field that the targets occupy. For cases in which the row of targets

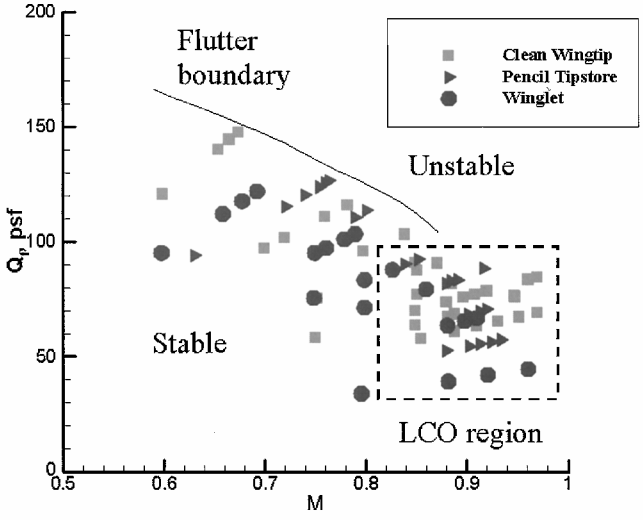

Fig. 4 Experimental test points for three wingtip configurations.

span nearly the entire image plane, sub-0.01 deg angular resolution is possible in the laboratory. Wind-tunnel angle-of-attack tests with precision inertial devices as the angular measurement reference indicate that 0.01-deg resolution can be achieved during wind-off tests and may be possible for wind-on tests, provided that the target row(s) occupy nearly the entire image plane and model translations while changing pitch are not excessive. However, the fraction of the image plane occupied by a target row near the wingtip may be less the 25% to image simultaneously the inboard portions of the wing and body. A typical angular resolution for model deformation measurements in the wind-tunnel environment may be 0.05 deg or larger near the wingtip due to the smaller fraction of the image plane occupied by the row of targets at the tip. A conservative estimate of the angular uncertainty for the data presented here is 0.05 deg. Displacement measurements in the laboratory have an uncertainty approaching 0.025 mm with a precision of 0.003 mm, but displacement measurement uncertainty in large wind-tunnel facilities is generally 5–10 times worse than laboratory values. The displacement uncertainty for the data reported here is estimated to be 0.3 mm. A more detailed uncertainty analysis of the VMD technique may be found in Ref. 4.

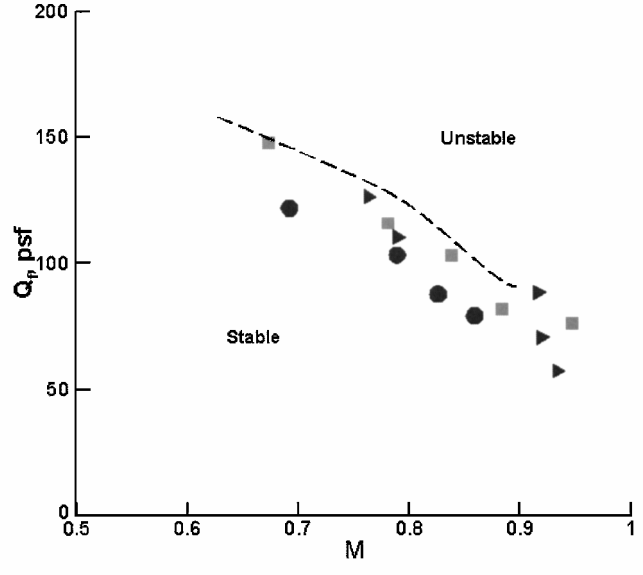

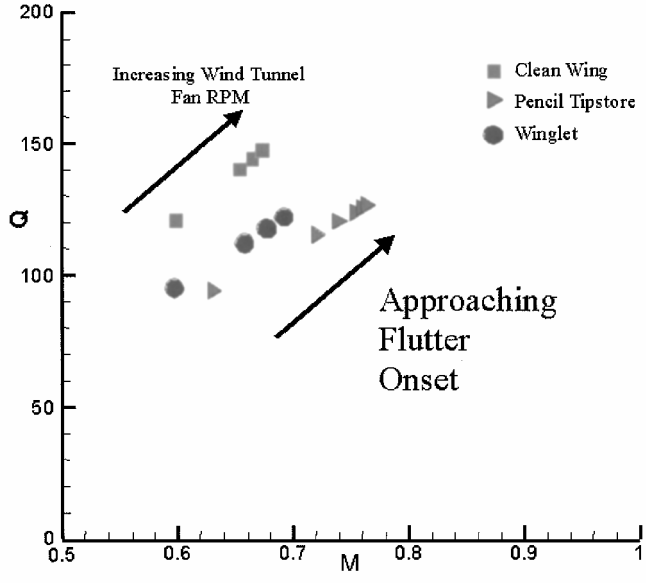

Fig. 6 Example of test points approaching flutter boundary.

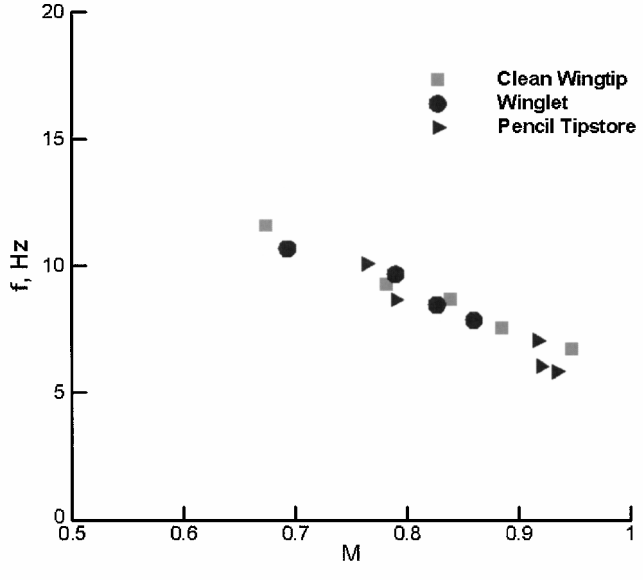

Fig. 5 Test points at approximate flutter boundary and frequencies in heavy gas: – – –, boundary and symbols, frequencies.

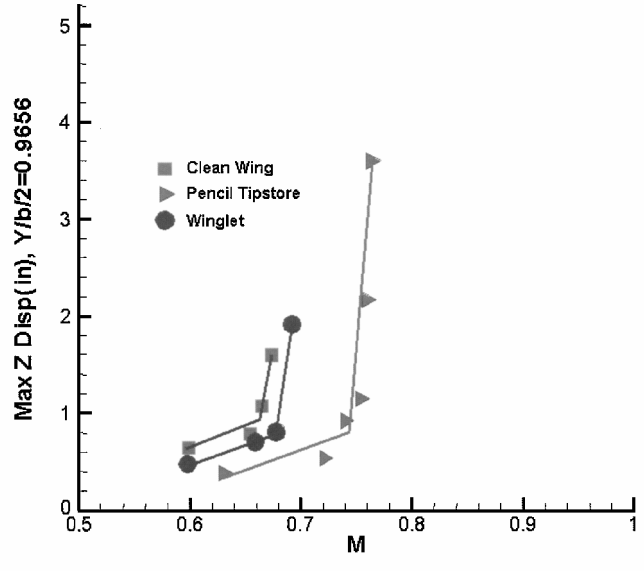

Fig. 7 Maximum peak-to-peak displacement at semispan = 0.9656 vs Mach number.

Results

For all previous tests with the videogrammetric system, the primary objective has been the measurement of static model and component deformation, not flutter and LCO dynamic measurements. The objective of this evaluation test was to assess the value of videogrammetric data during flutter and LCO testing and to determine operational characteristics and capabilities that might prove valuable in future measurement systems. A secondary objective was to obtain additional experience with videogrammetric techniques for dynamic measurements as part of an overall program to develop a videogrammetric dynamic (up to 1000 Hz) measurement capability.

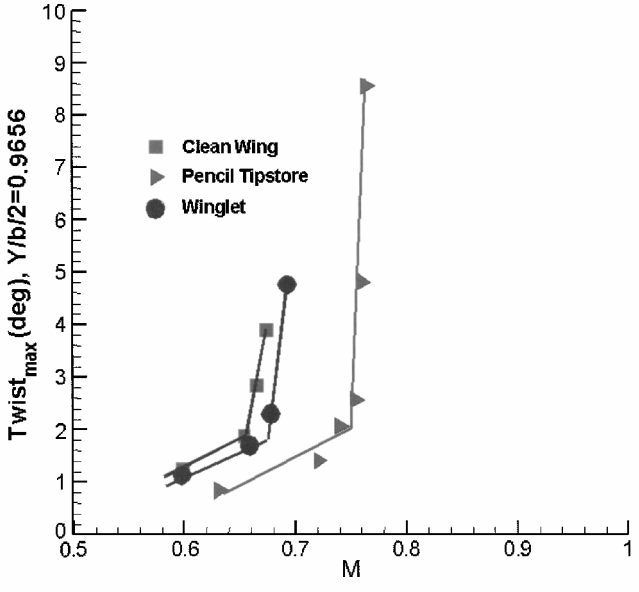

Fig. 8 Maximum peak-to-peak twist at semispan = 0.9656 vs Mach number.

For the portion of the test during which the videogrammetric system was operated, data were taken over a dynamic pressure Q range of 30–150 psf, a Mach number M range of 0.6–0.96, and at nominal model pitch angles α of -0.4, 0.6, 1.6, and 2.0 deg in heavy gas (R134a) mode only. Most of the videogrammetric data were acquired at $\alpha = 0.6$ deg; thus, results presented here are mainly for that model pitch angle. Measurements were made with three wingtips: clean, pencil tipstore, and winglet. Initially 6-s records at 60 images per second (yielding 360 images per point) were acquired at each data point. The time to process fully 360 images was typically 2 min and 20 s. The major portion of the processing time was expended in the image processing to extract centroid image plane coordinates of the 15 target locations for each image. The portion of the automated data reduction to convert from pixels to units of length (via photogrammetry) took only a few seconds. Later in the test, the time records were reduced to 5 s (300 images). For some selected data points only 2 s (120 images) of data were taken to reduce the time between points, but with reduced fidelity of the temporal recordings. The fully automated data results were output to several text data files. All of the files have header information to describe fully the data columns. An append file with X, Y, and Z mean coordinates for the 15 targets on the wing for each data point served as a summary data file for the mean coordinates. A text data file was also created for each data point that contained the X, Y, and Z data as a function of time for all 15 targets for that particular data point. Note that the Y value in these files was not computed, but was based on known target locations. Another file was created that contained the wing twist angle and vertical Z displacement for each of the five rows of targets as a function of time. Still another file was created that recorded tunnel data via a network data link for each data point recorded by the videogrammetric system.

Summary plots of the dynamic pressure–Mach number test space for $\alpha = 0.6$ deg data are presented in Figs. 4 and 5. The approximate

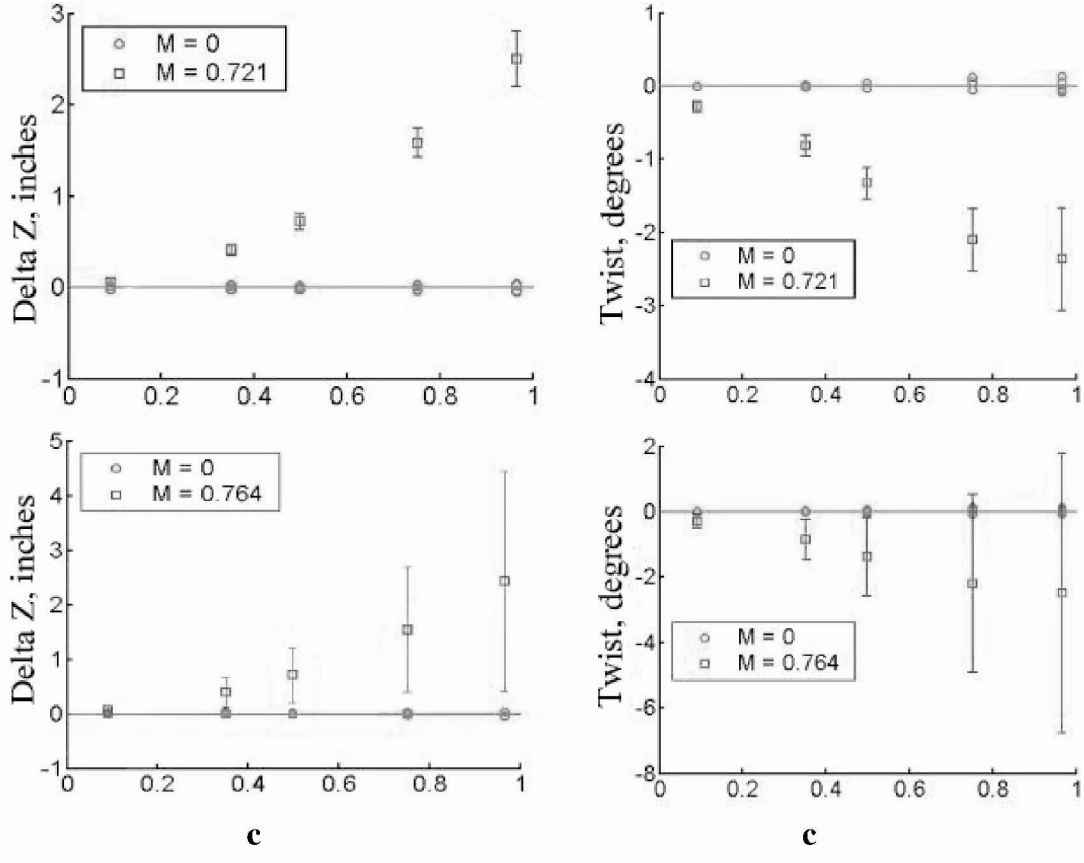

Fig. 9 Twist and bending with peak-to-peak ΔZ and $\Delta\theta$ as error bars for points near and far from flutter boundary.

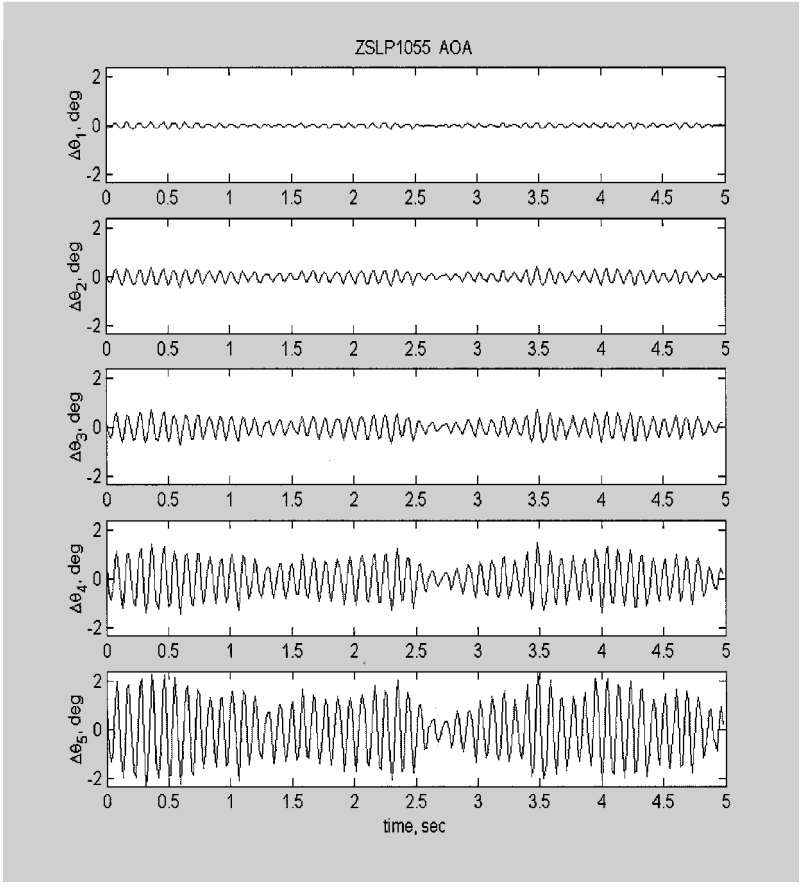

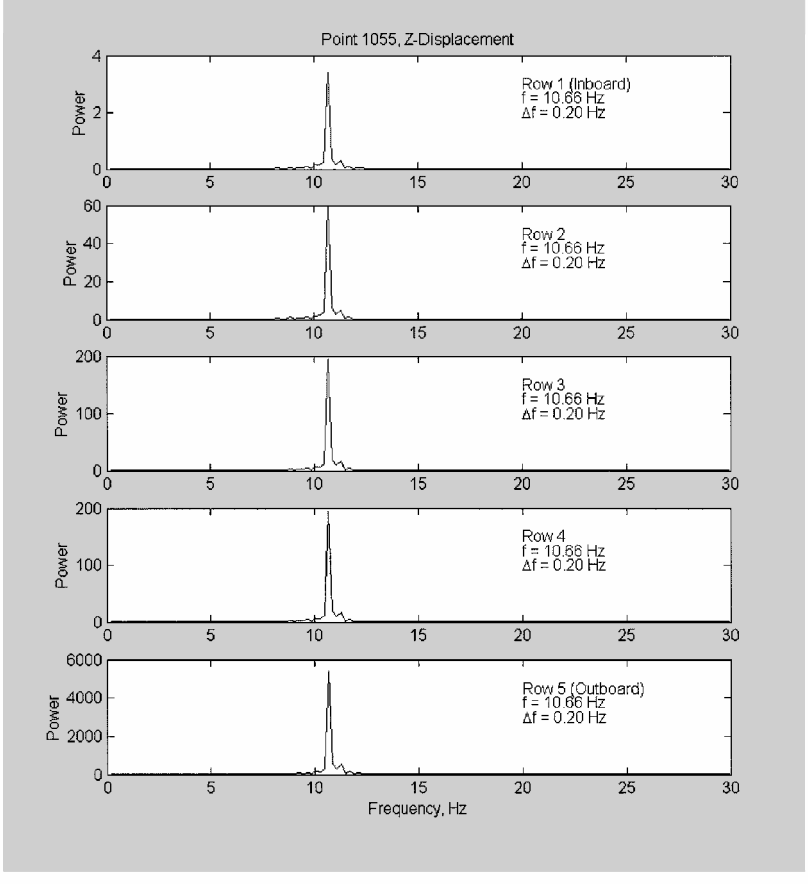

Fig. 10 Frequencies for five rows of targets and corresponding $\Delta\theta$ vs time.

flutter boundary and nearby data points representing the maximum Q and M where near flutterlike behavior occurs is illustrated in Fig. 4. Note that for flutter testing, tunnel pressure is held constant and that the test section Mach number and dynamic pressure are increased together by slow increases in the wind-tunnel fan speed. For flutter/LCO testing, the data points are generally started reasonably far from the estimated flutter boundary with Q and M being slowly and cautiously increased (and roughly perpendicular to the boundary) toward the flutter boundary. The arrows in Fig. 6 illustrate the path of the Q–M sweep toward the flutter boundary for three such cases. As the testing conditions reach the flutter boundary, excessive acceleration measurements of the model is noted and a bypass switch can be manually thrown by an experienced operator to reduce quickly tunnel conditions to below the point where flutter occurs to prevent damage to the model. However, the videogrammetric system was not automatically triggered by the bypass switch; thus, no data were taken at bypass points and all data points at bypass are missing. It is expected that future versions of the measurement system will offer post-trigger options to allow for the possibility to acquire data for a reasonable amount of time before and after the bypass switch is thrown. Such temporal records slightly before, during, and after bypass may prove valuable for future flutter/LCO tests.

The videogrammetric system may be used as an indicator of onset of the flutter boundary to complement accelerometers that were placed near the tip at the leading and trailing edges of the wing. Plots of peak-to-peak ΔZ and $\Delta\theta$ are shown in Figs. 7 and 8 vs M for the point sequences plotted in Fig. 6. The rise in $\Delta\theta$ and ΔZ as M (and correspondingly Q) is increased toward the flutter boundary may be useful in a future real-time implementation of the videogrammetric technique to assist a trained operator or eventually even become part of an automatic bypass detection system.

Plots of twist and bending with peak-to-peak ΔZ and $\Delta\theta$ as error bars are shown in Fig. 9 for points near and far from the flutter boundary. Five wind-off points are also included in the plots. The mean wind-off data are subtracted from the wind-on data to obtain the twist and bending due to aerodynamic loads.

The frequency of the variation of ΔZ and corresponding $\Delta\theta$ vs time of the five target rows for a typical data point near the flutter boundary are plotted in Fig. 10. Frequency spectra are calculated by fast Fourier transforms of the 5-s records of each $\Delta\theta$ and ΔZ time history. It is found that the frequencies of all five rows on the wing from inboard at $\eta = 0.0916$ to outboard at $\eta = 0.9656$ are equal. The Nyquist frequency for these samples is 29.97 Hz based on a sampling frequency of 59.94 Hz. The value 59.94 Hz, instead of 60 Hz, is derived from the standard pixel clock frequency of 14.31818 MHz common to RS-170 cameras. (The use of 59.94 Hz sampling instead of 60 Hz may lead to low-frequency beating in gray scale between the light source at a nominal 60-Hz frequency and the camera frequency.) The spectral resolution is 0.20 and 0.17 Hz for the 5- and 6-s records, respectively. Dynamic deformation contours for the first five images in a sequence are plotted in Fig. 11.

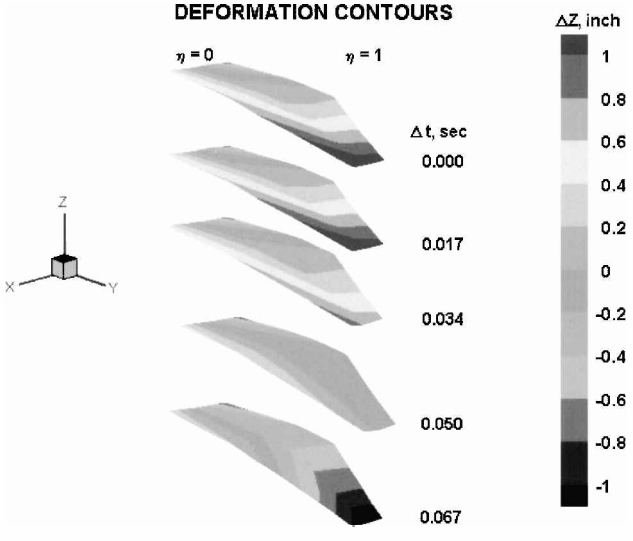

Fig. 11 Deformation contours for the first five images in a sequence.

Table 2 D_{max} as determined by accelerometer and videogrammetric data for dynamic pressure Q and Mach number M

D_{max}, in			
Accelerometer	Videogrammetric	Q, psf	M
0.82	0.58	123.6	0.754
0.89	1.08	125.4	0.760
1.68	1.80	126.4	0.764

Comparisons of half-amplitude determined with the videogrammetric measurement system at $\eta = 0.9656$ and with accelerometer data at $\eta = 0.90$ are given in Table 2. Differences in the measured data occur because the accelerometer and the videogrammetric measurement system are not at identical locations. The maximum displacement D_{max} of the accelerometer data is computed assuming sinusoidal oscillations from

$$D_{max} = a/4\pi^2 f^2 \tag{5}$$

where a is the acceleration and f is the frequency. The peak acceleration for the accelerometer data was estimated from time history plots by hand fitting a line through the approximate average peak of the traces. This process, in addition to spectral energy at other than the peak frequency, is estimated to cause an uncertainty in the peak displacement of up to 0.1 in. or more when calculated from the accelerometer data. At lower peak-to-peak oscillations, the bias error in the accelerometer data increases and typically results in a larger computed value of peak displacement when compared to the videogrammetric data as noted for the data in Table 2 at $M = 0.754$.

Conclusions

The application of videogrammetric techniques is shown to be a viable alternative technique to accelerometers for the measurement of dynamic displacements during LCO testing. Accurate measurement of the wing motion during flutter and LCO testing is critical when comparing unsteady surface pressures with computed results. Modern CAE programs are capable of simultaneously computing both the vehicle motion and dynamic loads on the vehicle. However, accurate simultaneous computation of these components is difficult for highly nonlinear problems such as LCO, and it is beneficial to be able to isolate the various components of the problem. By the specification of the model motion using data obtained with videogrammetry, the issue of computing the model motion can be eliminated from the computational problem, and a direct comparison of computed and wind-tunnel pressures can be performed. Videogrammetry provides a significantly more accurate, direct, and relatively low-cost method for obtaining these crucial data and appears to be a very useful complement to accelerometer data for future flutter and LCO testing. In addition, videogrammetric techniques offer the promise of direct comparisons of computed and wind-tunnel pressures without the additional need to compute the model motion.

References

[1]Bunton, R. W., and Denegri, C. M., Jr., "Limit Cycle Oscillation Characteristics of Fighter Aircraft," *Journal of Aircraft*, Vol. 37, No. 5, 2000, pp. 916–918.

[2]Denegri, C. M., Jr., "Limit Cycle Oscillation Flight Test Results of a Fighter with External Stores," *Journal of Aircraft*, Vol. 37, No. 5, 2000, pp. 761–769.

[3]Edwards, J. W., Schuster, D. M., Spain, C. V., Keller, D. F., and Moses, R. W., "MAVRIC Flutter Model Transonic Limit Cycle Oscillation Test," NASA TM 210877, May 2001.

[4]Burner, A. W., and Liu, T., "Videogrammetric Model Deformation Measurement Technique," *Journal of Aircraft*, Vol. 38, No. 4, 2001, pp. 745–747.

[5]Liu, T., Radeztsky, R., Garg, S., and Cattafesta, L., "A Videogrammetric Model Deformation System and Its Integration with Pressure Paint," AIAA Paper 99-0568, 38th Aerospace Sciences Meeting, Reno, NV, Jan. 1999.

[6]Burner, A. W., Liu, A., Garg, S., Ghee, T., and Taylor, N., "Aeroelastic Deformation Measurements of Flap, Gap, and Overhang on a Semispan Model," *Journal of Aircraft*, Vol. 38, No. 6, 2001, pp. 1147–1154.

[7]Burner, A. W., Wahls, R. A., and Goad, W. K., "Wing Twist Measurements at the National Transonic Facility," NASA TM 110229, Feb. 1996.

[8]Graves, S. S., and Burner, A. W., "Development of an Intelligent Videogrammetric Wind Tunnel Measurement System," Proc. SPIE Vol. 4448, Optical Diagnostics for Fluids, Solids, and Combustion, SPIE—The International Society for Optical Engineering, Nov. 2001, pp. 120–131.